UNIVERSITY OF CALIFORNIA, SAN DIEGO

Investigation into the function of a novel protein, PHR, in regulating *Dictyostelium discoideum* chemotaxis

A Thesis submitted in partial satisfaction of the
requirements for the degree of Master of Science

in

Biology

by

Ashley Marie Lakoduk

Committee in charge:

Professor Richard A. Firtel, Chair
Professor Steven P. Briggs
Professor Colin Jamora

2012

This Thesis of Ashley Marie Lakoduk is approved and it is acceptable in quality and form for publication on microfilm and electronically:

Chair

University of California, San Diego

2012

TABLE OF CONTENTS

LIST OF FIGURES

LIST OF SUPPLEMENTAL FILES

ACKNOWLEDGEMENTS

I would like to acknowledge Professor Richard Firtel for his support as the chair of my committee. His mentorship has proven to be invaluable, both within and outside of the laboratory setting.

I would also like to thank the members of the Firtel lab for their support in my pursuit of this degree. I would like to specifically acknowledge Pascale Charest. Without her guidance I would never have been able to complete this work. She has proven to be pivotal in my experience as a graduate student, and no words are sufficient to express my appreciation for all that she has done.

Additionally, I would like to acknowledge Pascale Charest, Zhouxin Shen, Atsuo T. Sasaki, Steven P. Briggs, and Richard A. Firtel, co-authors with me of "A Ras Signaling Complex Controls the RasC-TORC2 Pathway and Directed Cell Migration" published in *Developmental Cell* May 18th, 2010, which contains, in part, research presented in this Thesis.

ABSTRACT OF THE THESIS

Investigation into the function of a novel protein, PHR, in regulating *Dictyostelium discoideum* chemotaxis

by

Ashley Marie Lakoduk

Master of Science in Biology

University of California, San Diego, 2012

Professor Richard A. Firtel, Chair

In a study by Charest et al., 2010 a protein signaling complex was discovered and found to regulate the RasC-TORC-PKB/PKBR1 pathway at the leading edge of chemotaxing *Dictyostelium discoideum* cells. A novel protein, PHR, is a stable member

of this Sca1 protein complex. This present study is an in-depth analysis of *phr* null strains in the regulation of chemotaxis in *Dictyostelium* cells.

Analyses of phr knockout cells show clear alteration of actin and myosin cytoskeleton dynamics as well as altered cell motility. Though it was discovered that PHR is a stable member of the Sca1 protein signaling complex, it does not affect RasC activity. Intriguingly, *phr* knockout does seem to modulate the downstream TORC2-mediated phosphorylation of PKB and PKBR1 proteins, despite having no observed effect on RasC activity. Thus, additional roles for PHR in regulating chemotaxis outside of the Sca1 complex was proposed. However, due to the fact that the correct topology of the PHR gene is currently unknown, attempts to generate cells expressing epitope-tagged PHR to test for alternative roles in chemotaxis regulation has proven unsuccessful. The exact functions of PHR in the spatiotemporal regulation of chemotaxis remains unclear.

I. INTRODUCTION

What is chemotaxis?

Chemotaxis, or directed cell migration, is the ability of cells to detect and move towards an external chemical stimulant. The ability for cells to migrate is essential for numerous cellular processes including: embryonic development, the immune and inflammatory responses, as well as the metastasis of tumor cells. Biological studies using the organism *Dictyostelium discoideum* have advanced our understanding of the intracellular signaling mechanisms that spatiotemporally regulate chemotaxis.

Dictyostelium discoideum as a Model Organism

Dictyostelium discoideum is a soil-dwelling eukaryotic social amoeba that undergoes chemotaxis in nature. In response to folate in the surrounding environment, secreted by its bacterial food source, *Dictyostelium* initiates a chemotaxis response to track down its prey (King and Insall, 2009). Additionally, under starvation conditions, *Dictyostelium* will secrete cyclic adenosine monophosphate (cAMP), a communicative signal to surrounding unicellular *Dictyostelium* to initiate a development program, resulting in the formation of hardy fruiting bodies as a mechanism of survival until food sources become available (Chisholm and Firtel 2004). cAMP is a chemoattractant that is produced locally through a process called signal relay, leading to the formation of *Dictyostelium* aggregates.

In addition to its innate chemotaxis program, *Dictyostelium* is also a useful model organism because its haploid genome has been fully sequenced (Eichinger et al., 2005),

making the generation and isolation of genetic mutants easily feasible. Additionally, *Dictyostelium* is readily cultured in the laboratory setting. Most importantly, it has been found that the *Dictyostelium* genome has many genes that are homologous to higher Eukaryotes (Kortholt and Van Haastert 2008). Thus, experimentation with *Dictyostelium discoideum* is a convenient means for gaining insight into conserved cellular processes in higher multicellular organisms.

Chemotaxis is a Culmination of Concerted Processes: Directional Sensing, Cytoskeleton Rearrangement, Cell Polarity and Cell Motility

Studies performed in *Dictyostelium* have shed light on the complex intracellular processes regulating directed cell migration. To initiate chemotaxis, the chemoattractant cAMP binds to a transmembrane cAMP receptor (cAR) that is uniformly distributed over the cell surface of the *Dictyostelium* cell (Xiao et al., 1997). These cAR proteins are associated with intracellular heterotrimeric G proteins, making these cAMP receptors G-protein coupled receptors (GPCRs). These heterotrimeric G proteins consist of alpha (α), beta (β), and gamma (ɣ) subunits and are also uniformly distributed over the cell surface (Jin et al., 2000). These G proteins dissociate and activate upon cAR stimulation and act intracellularly to bias the cell in the direction of the cAMP signal (Figure 1).

Cells achieve cell polarity, having a distinct front and rear, through the establishment of a steep intracellular gradient of the signaling molecule phosphatidylinositol (3,4,5)-triphosphate ($PI(3,4,5)P_3$). As seen in Figure 1, $PI(3,4,5)P_3$ is generated at the leading edge of cells through the phosphorylation of phosphatidylinositol (4,5)-biphosphate ($PI(4,5)P_2$) by the protein phosphoinositol 3-kinase (PI3K). The steep

internal gradient is maintained by the dephosphorylation of $PI(3,4,5)P_3$ by phosphatase tensin homologue (PTEN) to $PI(3,4,5)P_2$ at the rear and lateral sides of the cell (Ijima and Devreotes 2002). This localized accumulation of $PI(3,4,5)P_3$ at the leading edge promotes the cytoskeleton rearrangement necessary for cellular migration via the recruitment and docking of other pleckstrin homology (PH)-domain containing proteins to the leading edge, such as Akt/protein kinase B (PKB). Akt/PKB and other proteins that are recruited to the leading edge via $PI(3,4,5)P_3$ accumulation guide the localized polymerization of filamentous actin (F-actin), resulting in pseudopod extension (Cenni et al., 2003; Affolter and Weijer, 2005). F-actin polymerization acts as a positive feedback mechanism to recruit more PI3K to the plasma membrane at the leading edge of cells (Charest and Firtel, 2007).

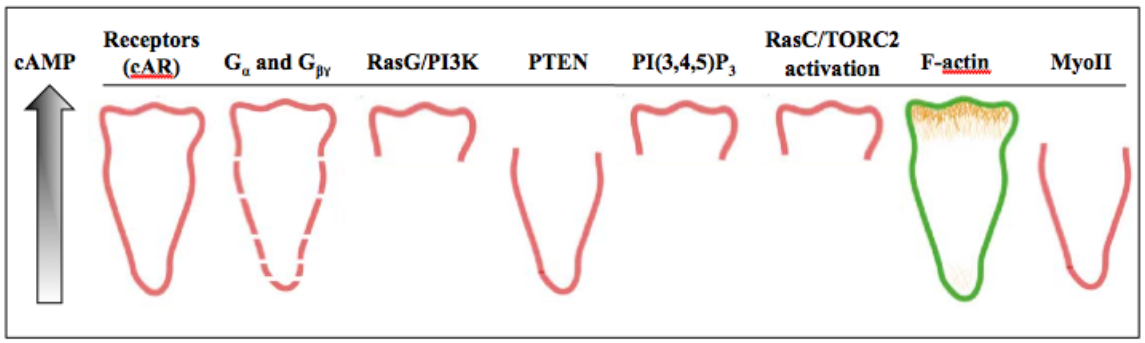

Figure 1. Cellular distribution of signaling molecules. Localization of different signaling molecules within a polarized *Dictyostelium* cell in response to extracellular cAMP gradient. Figure adapted from Sasaki and Firtel (2006).

Interestingly, though $PI(3,4,5)P_3$ has been shown to be a major regulator of cytoskeleton dynamics (Kölsch et al., 2008; Sasaki et al., 2006), studies have proven that $PI(3,4,5)P_3$-independent chemotaxis is possible and occurs through the activation of a protein complex, target of rapamycin complex 2 (TORC2), at the leading edge of

chemotaxing cells (Lee et al., 2005; Kamimura et al., 2008; Charest et. al, 2010). The *Dictyostelium* TORC2 complex is comprised of a Tor kinase associated with Pia, Rip3, and Lst8 subunits. These subunits are orthologs of mammalian Rictor, mSin1, and mLst8, respectively (Lee et al., 2005). The major known biochemical role for TORC2 is the activation of two Akt homologues, PKB and PKB-related PKBR1, through the phosphorylation of their hydrophobic motifs (HM) (Sarbassov et al., 2005; Kamimura et al., 2006). As mentioned previously, PKB is a known regulator of cytoskeleton dynamics through the polymerization of F-actin.

The cumulative product of the intracellular signaling in polarized *Dictyostelium* cells is the generation of a motile cell through the protrusion of pseudopods at the leading edge and the retraction of the rear of the cell. The protrusive forces needed for pseudopod formation are generated by the regulated F-actin polymerization at the front of the cell. Similarly, retractive forces at the rear of the cell are achieved by the regulation of myosin II motors (Mondal et al., 2008). At the leading edge of chemotaxing cells, a Ras-like GTPase, Rap1, is activated in response to cAMP. Rap1 helps cells achieve cell polarity through regulating Myosin II assembly/disassembly by modulating the downstream phosphorylation of Myosin II (Charest and Firtel, 2007; Jeon et al., 2007). This F-actin-dependent phosphorylation of Myosin II causes its dissociation from the leading edge of the cell and the subsequent localization of Myosin II at the rear and lateral sides. There, Myosin II functions to prevent the formation of lateral pseudopodia in the cell (Chung and Firtel, 2000). Both actin polymerization and Myosin II activity are tightly regulated through the intracellular signaling of small, monomeric G proteins (Bolourani et al., 2006; Charest and Firtel, 2007).

Ras Signaling

Ras signaling is the earliest implicated mode of intracellular signal amplification, directly activated downstream of the chemoattractant receptor and heterotrimeric G proteins (Sasaki et al., 2004). Ras proteins are small, monomeric G proteins (Bourne et al., 1991). These Ras proteins act as molecular switches, cycling between active (GTP-bound), and inactive (GDP-bound) states (Figure 2). Activation is regulated by guanine-nucleotide exchange factors (GEFs or RasGEFs) and deactivation is facilitated through the hydrolysis of the bound GTP to GDP, catalyzed by GTPase-activating proteins (GAPs or RasGAPs) (Boguski and McCormick, 1993).

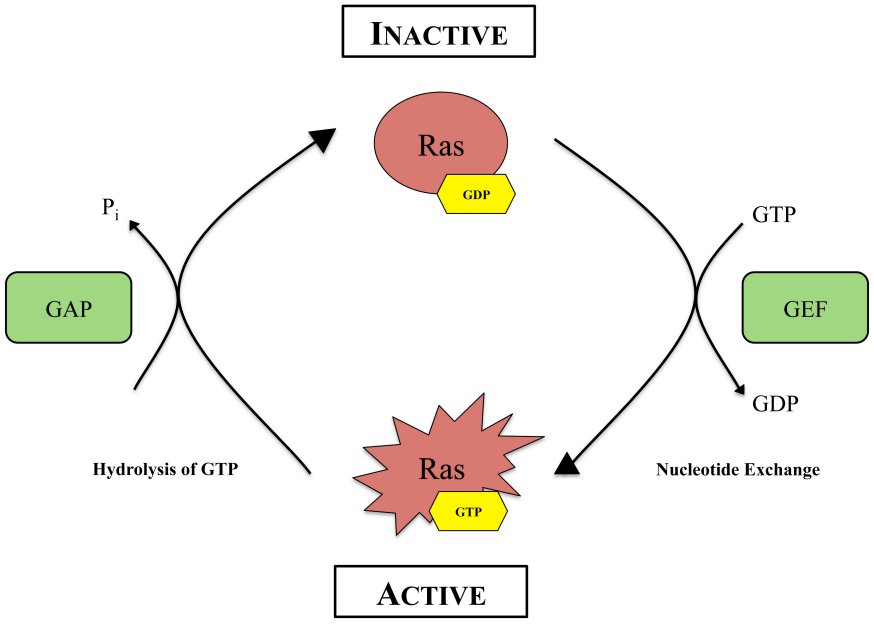

Figure 2. Ras as a molecular switch. The activity of Ras proteins is controlled by a cycle of nucleotide exchange and hydrolysis. RasGEFs facilitate the dissociation of GDP from inactive Ras, promoting Ras activation. RasGAPs catalyze the hydrolysis of GTP in active Ras proteins, negatively regulating Ras proteins. P_i, inorganic phosphate.

Ras proteins were first implicated in *Dictyostelium* chemotaxis through the generation of a mutant named Aimless (protein: RasGEFA, gene: *aleA*), a homologue of the mammalian RasGEF SOS (Son of Sevenless), in which chemotaxis and cAMP production was impaired (Insall et al., 1996; Lee et al., 1999). These studies suggested that this RasGEF was important in regulating chemotaxis and signal relay, alluding to the idea that these processes are controlled upstream by the Ras family of small GTPases.

The Ras superfamily can be divided into several subfamilies based on distinct sequences (Colicelli, 2004). The most important subfamily for this present study is the Ras subfamily. The *Dictyostelium* genome encodes a multitude of Ras subfamily GTPases (Weeks et al., 2005). Though there is much overlap in function between the subfamily members, there is evidence for Ras-specificity in different cellular processes (Weeks and Spiegelman, 2003; Rodriquez-Viciana et al., 2004). Two Ras proteins, RasC and RasG, were found to be activated in response to cAMP. In a study by Bolourani et al., distinct functions were noted for RasC and RasG: RasG is implicated in regulating the cytoskeleton through PI3K activity, while RasC is the major regulator of adenylyl cyclase A (ACA) activity and signal relay. RasC regulates signal relay through its modulation of the TORC2-mediated phosphorylation of PKB/PKBR1 and downstream ACA activity, controlling the production of cAMP (Charest et al., 2010). Though chemotaxis is controlled by several distinct pathways, one fact remains clear: for TORC2 activity and $PI(3,4,5)P_3$ accumulation at the leading edge of cells, there must be tight intracellular regulation of Ras proteins.

Sca1 Complex Controls the RasC/TORC2 Pathway at the Leading Edge

In a study by Charest et al., a protein signaling complex was found to control RasC activation at the leading edge of chemotaxing cells. This complex is comprised of two RasGEFs, Aimless/RasGEFA and RasGEFH; the structural A subunit of protein phosphatase2A (PP2A-A); a new putative catalytic C subunit of PP2A (PP2A-C2); and two previously uncharacterized proteins of molecular weight 174.9 kDa and 111.6 kDa. These proteins were later named Sca1 and PHR, respectively (Figure 3). These proteins were identified using proteomics when looking for proteins that interact with Aimless/RasGEFA in a pull-down experiment using epitope-tagged RasGEFA in *gefA*$^{-}$ cells (Figure 4).

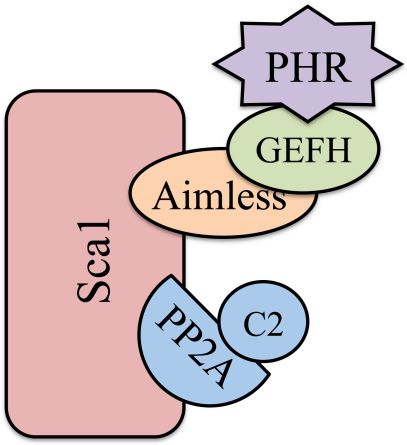

Figure 3. Sca1 Protein Complex. Experimentally-derived architecture of the Sca1 protein complex by Charest et al., 2010. Complex components include: a protein scaffold (Sca1), two Ras guanine exchange factors (Aimless and RasGEFH), protein phosphatase 2A (PP2-A), a new catalytic subunit of PP2A (PP2A-C2), and a novel protein, PHR. Figure adapted from Charest et al., 2010.

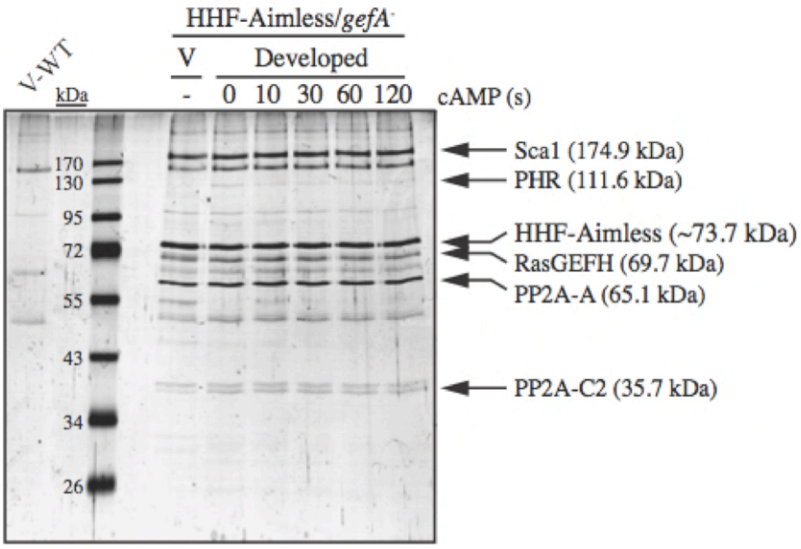

Figure 4. PHR is part of a multi-protein complex. Silver staining of the SDS-PAGE-resolved proteins pulled-down by sequential His-Flag purification using HHF-Aimless as bait expressed in *gefA*$^-$ cells from either vegetative (V) or developed cells stimulated or not with 1µM cAMP for the time indicated. Wild-type cells (WT; AX2) used as control. The purified proteins were identified using mass spectrometry, and their respective molecular weights are indicated. Figure taken with permission from Charest et al., 2010.

The same study later found that these proteins form a stable complex that regulates chemotaxis and signal relay through the direct control of RasC activity, via the GEF activity of a RasGEFA:RasGEFH heterodimer. Active RasC in turn modulates the downstream TORC2-mediated phosphorylation of PKB/PKBR1 at their hydrophobic motifs at the leading edge (Figure 5). The Sca1 complex regulation of the RasC/TORC2 pathway was also proven to be PI(3,4,5)P_3-independent. The study by Charest et al., also noted that tight spatiotemporal regulation of Ras activity was key for chemotaxis and signal relay, as a negative feedback loop was proposed (Figure 5).

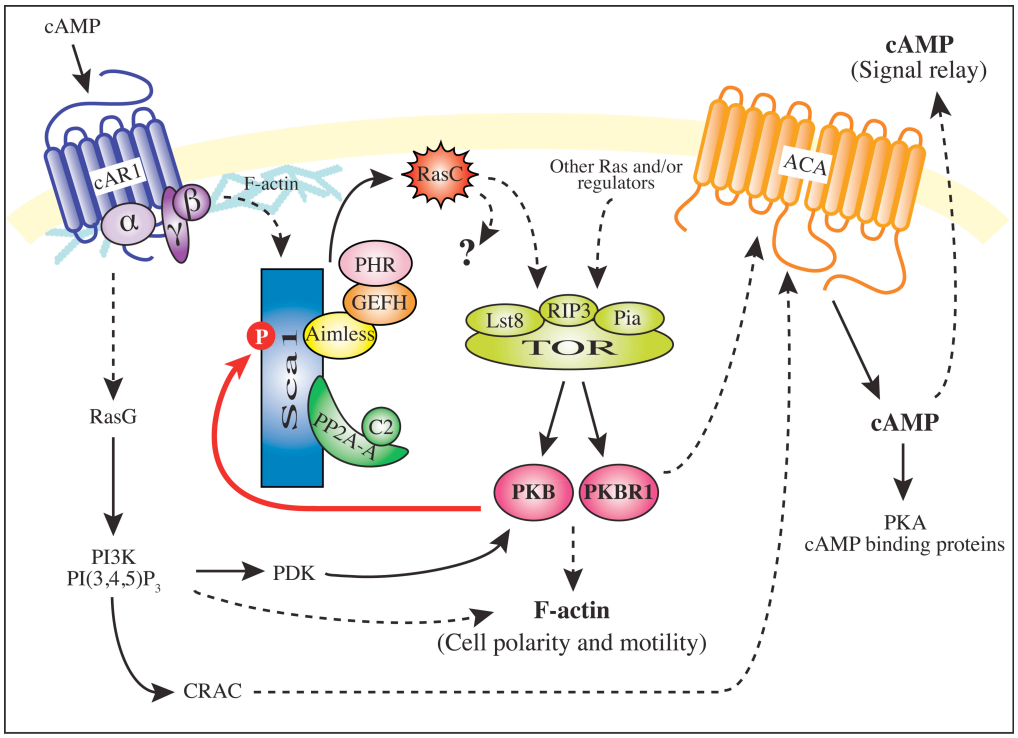

Figure 5. Regulation of RasC in *Dictyostelium*. Proposed by Charest et al., 2010: the Sca1 complex is recruited to the plasma membrane upon chemoattractant stimulation, resulting in the activation of the RasC-TORC2-PKB/PKBR1 pathway through the Aimless:RasGEFH heterodimer, regulating signal relay and cell motility. Observations by Charest et al., 2010 also suggest that PKB/PKBR1 regulates RasC activity in a negative feedback loop, possibly through direct phosphorylation modifications to the Sca1 complex. Figure taken with permission from Charest et al., 2010.

An Introduction to PHR

PHR was identified as a stable member of the Sca1 protein signaling complex. PHR is recruited to the Sca1 complex through interactions with the protein RasGEFH (Charest et al., 2010). PHR is a 111.6 kDa protein with two major protein domains: a PH domain and a Ras GTPase domain (Figure 6). The major functions of a PH domain is intracellular signaling, through binding of inositol phosphates, phosphatidylinositol lipids, cytoskeleton components, or other protein binding. The major function of PHR's other protein domain, a Ras GTPase domain, is to hydrolyze GTP. There is sequence

similarity between the GTPase domain of PHR and other Ras superfamily small GTPases, however with an ill-defined subfamily (*smart.embl-heidelberg.de*).

Figure 6. SMART Protein domains of PHR. Diagram showing PHR protein domain composition and organization as predicted by SMART databases. PH, Plectstrin homolgy domain; pink segments are regions of low complexity.

II. RESULTS

Generation of a PHR knockout strain in *Dictyostelium*

In order to characterize the role of PHR in *Dictyostelium* development and chemotaxis, a knockout was generated using the construct shown in Figure 7. PCR was used to generate two non-overlapping genomic sequences of PHR - PHR "A" and "B." Fragment PHR "A" is downstream of the genomic start (ATG) site, and PHR "B" ends just upstream of the gene termination (TAA) sequence. These two fragments were then cloned into a pBluescript (pBS) SK- vector along with a Blasticidin S-resistance (BSR) cassette in order to disrupt the PHR gene via homologous recombination. This PHR-A(BSR)B-pBS construct was sequenced for accuracy and linearized using restriction enzymes KpnI and NotI before transformation into *Dictyostelium* (see Materials and Methods).

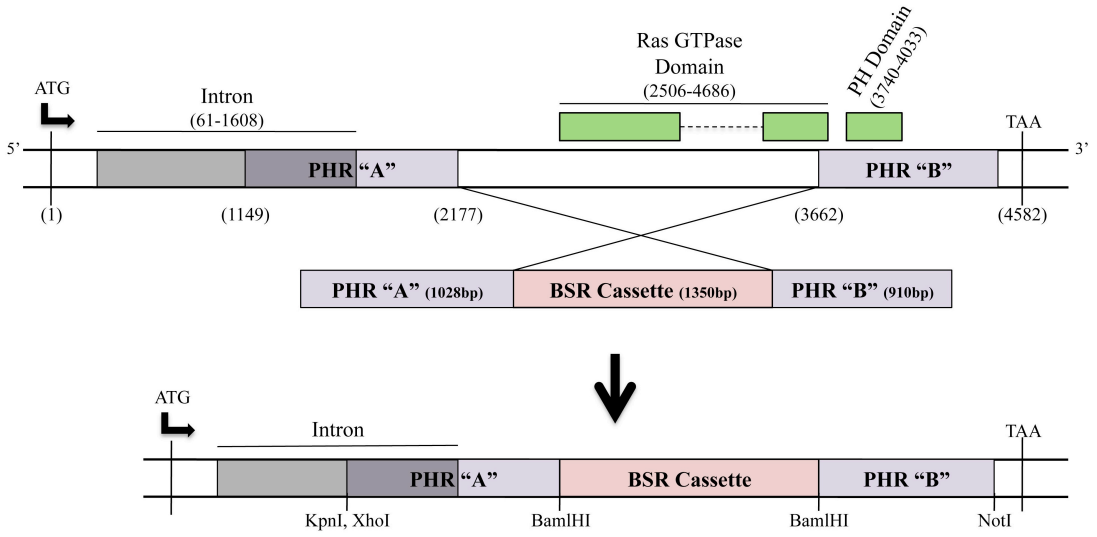

Figure 7. Representation of the *phr* knockout construct. Representation of homologous recombination between linear PHR-A(BSR)-B knockout construct and PHR genomic DNA (gDNA). Exact nucleotide positions for each fragment of DNA, intron, and corresponding protein domains, as well as start (ATG) and stop (TAA) sequences are shown.

After transformation into *Dictyostelium* via electroporation, the cells were selected using Blasticidin-selective HL5 media and cloned on bacterial lawn. Twenty-four clones were isolated and screened using PCR (Figure 8). The initial PCR screen amplified the N-terminus of the gene knockout using primers PC136 and BSR 5'Out, which hybridize within the construct at the beginning of Fragment PHR "A" and within the BSR cassette in the 5' region, respectively (Figure 8A). The initial PCR screen results are shown in Figure 8B, along with the PHR-A(BSR)B-pBS plasmid and WTgDNA as positive and negative controls, respectively. A 1.6kb band is expected using primers PC136 and BSR 5' Out in strains where the gene was successfully disrupted, and is indicated in the figure by a bold arrow. Positive strains are underlined. A second PCR Screen was performed to amplify the C-terminus of the gene knockout using primers that hybridize in the 3' region of the BSR cassette (BSR 3' Out) and the C-terminal region of the PHR "B" fragment (PC139). Results of this PCR Screen are shown in Figure 8C, where positive clones are expected to be 1.1kb in size and are underlined. Both the positive [PHR-A(BSR)B-pBS] and negative (WTgDNA) controls are shown in Figure 8C. Note that this PCR Screen shows high background in the controls, so another PCR screen was designed for better confirmation. The third PCR Screen, using a primer that hybridizes within the N-terminal genomic sequence of PHR (PC233) and primer BSR 5' Out, is shown in Figure 8D. This PCR screen shows less background and gives more conclusive evidence. This third PCR screen also confirms that the knockout construct was inserted into the correct location within the *Dictyostelium* genome as PC233 hybridizes outside of the sequence used to make the KO construct. Ten clones that were

positive for all three PCR Screens were chosen for further confirmation via Southern blotting and were re-named Clones 1-10 (Figure 8D, indicated in red).

For further confirmation that these clones were indeed true knockouts, a Southern blot was performed under two different conditions. Figure 9B shows an autoradiogram of the Southern Blot performed under the first condition. A ~2kb band is expected for wild-type DNA and a shift to ~3kb is expected if *phr* was successfully disrupted (Figure 9A). The bold arrows in Figure 9B show the expected positions of each band.

An autoradiogram of the second condition is shown in Figure 9C. In this condition, we expect a wild-type band at ~2kb, which should be absent in the knockout strains. As shown in Figure 9C, there is no observed band at 2kb for any of the potential knockout clones.

Though the Southern blot performed is not absolutely conclusive for the gene knockout, we concluded that the data was sufficient proof of *phr* knockout when coupled with the three PCR screens. For simplicity, all further discussion involving knockout cell lines will be denoted as phr^-. phr^- clone 8 (formerly clone 16 in the PCR Screens) was chosen for further characterization of the null phenotype and is noted via underlining in Figures 9B and C.

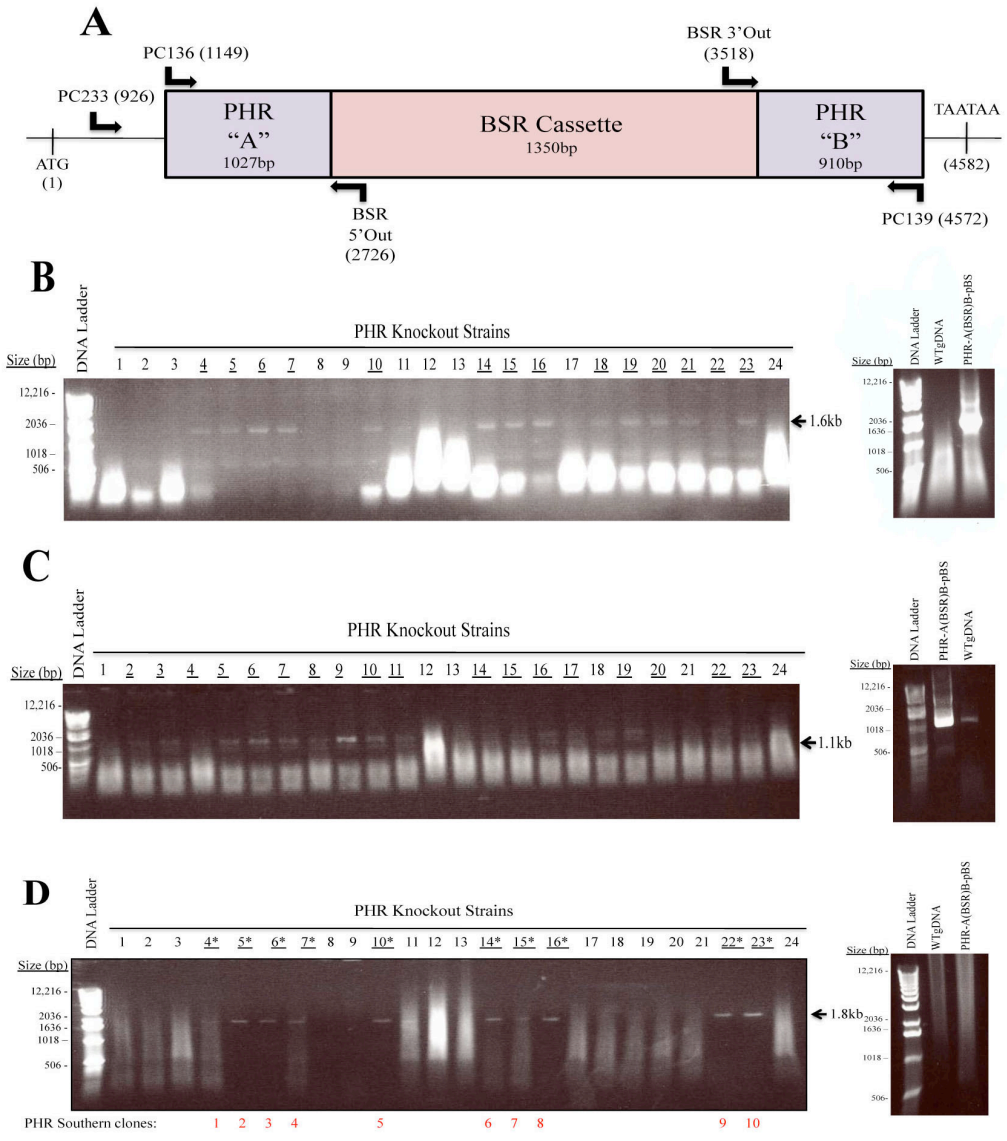

Figure 8. PCR Screens for *phr* knockout. (A) Representation of the PHR knockout construct. Arrows depict where the primers hybridize on the construct for PCR amplification and exact nucleotide sequence positions are denoted in parenthesis. **(B)** Initial PCR Screen of twenty-four (24) potential PHR knockout strains using primers PC136 and BSR 5' Out. **(C)** Second PCR Screen using primers PC139 and BSR 3' Out. **(D)** Third PCR Screen using primers PC233 and BSR 5' Out. All clones thought to be positive are underlined. Ten strains were chosen for further analysis and are indicated with asterisks. Corresponding numbers in Southern Blot are noted below, in red.

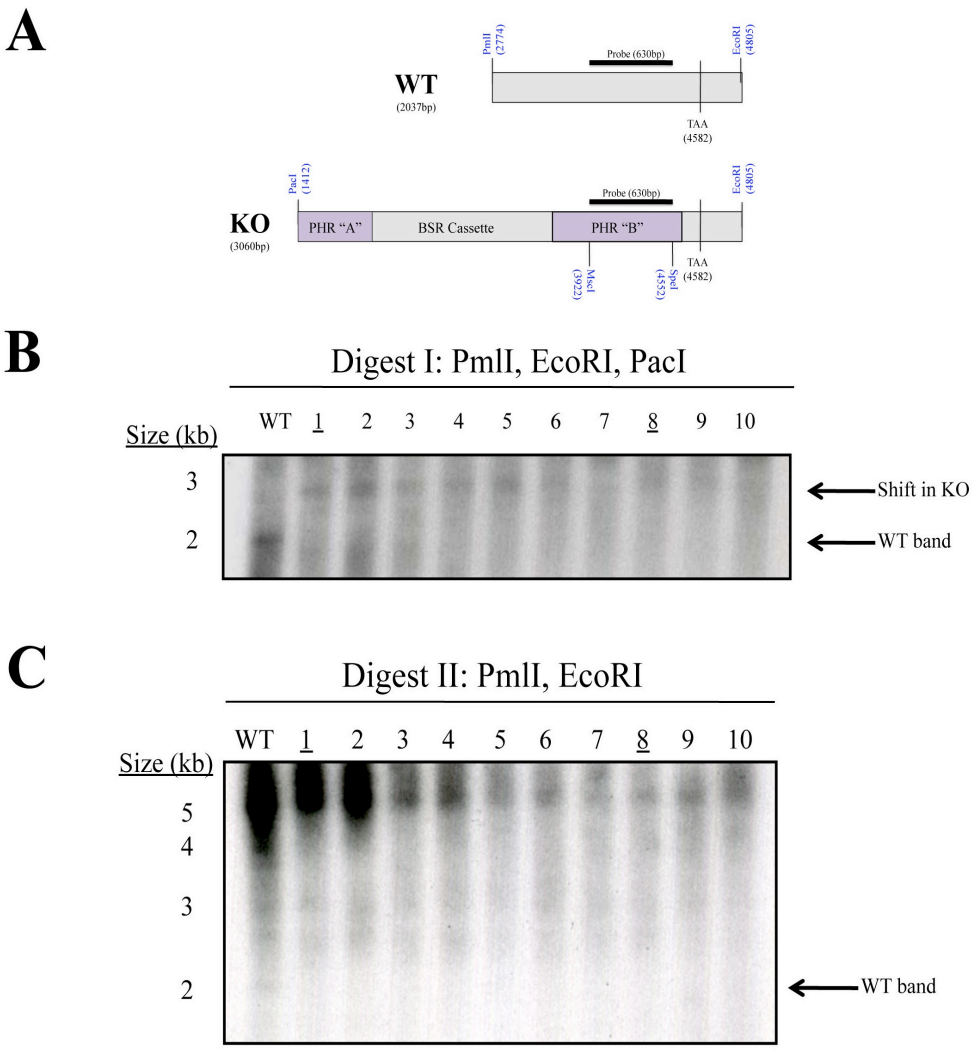

Figure 9. Southern blot for *phr* knockout confirmation. Clones were chosen after confirmation from three separate PCR screens before Southern blot and renamed 1-10. **(A)** Shows the expected sizes of the different bands in the First condition. MscI and SpeI restriction digested PHR fragment "B" was used as the probe (630 bp). **(B)** Autoradiogram of a Southern Blot performed under the first condition. Bold arrows indicate the size of the expected band in WT and knockout strains. **(C)** Autoradiogram of a Southern Blot performed under the second condition. Bold arrow indicates expected size of WT band.

phr⁻ cells display normal growth and cytokinesis

phr⁻ cells growing on plates appear larger than wild-type cells (data not shown). This could be due to the cells being flatter, more spread out, or to a cytokinesis defect. To test the possibility of the latter, analysis of *phr*⁻ cell growth and ability to undergo cytokinesis was assessed and compared to wild-type cells. Figure 10A shows a graph representing the growth curves of both wild-type and *phr*⁻ cells growing in suspension. As can be seen in the graph, *phr*⁻ cells grow at the same rate as wild-type cells.

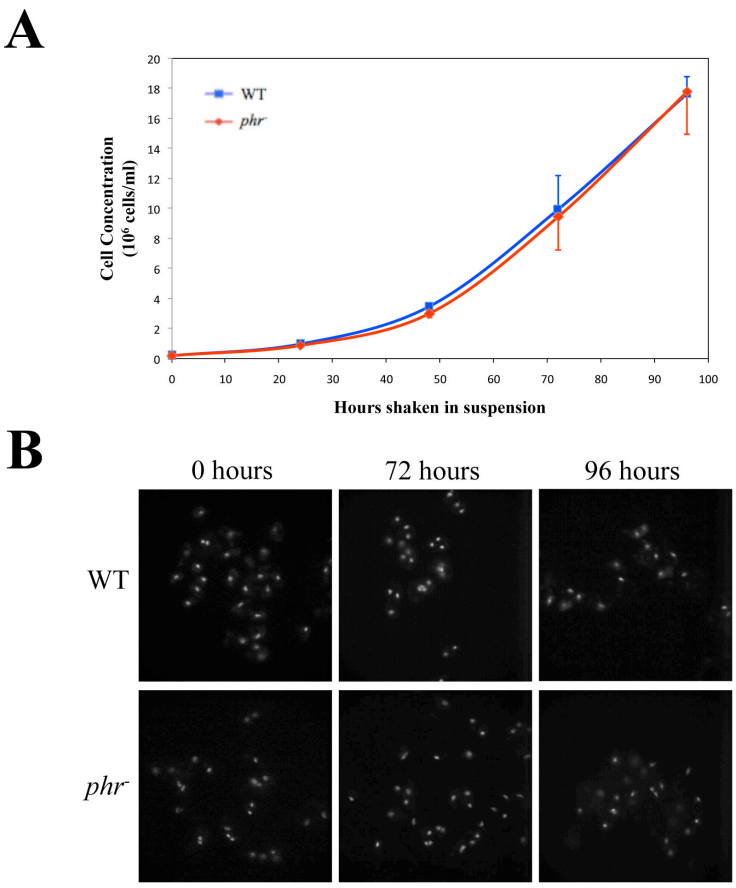

Figure 10. *phr*⁻ cell growth and cytokinesis. (A) Growth curves of WT and *phr*⁻ cell lines in suspension. Vertical error bars represent SEM. **(B)** Images of DAPI stained nuclei of *phr*⁻ cells compared with WT. Images of cells taken from plates before inoculation of shaking cultures (0 hours) and at 72 and 96 hours of growth in suspension. All Shaking cultures started at 0.2 x 10^6 cells/ml. All images taken at magnification of 63X. Data are representative of 4 independent experiments.

For further analysis of the knockout cell line's ability to undergo cytokinesis, DAPI staining of the cells' nuclei was done on *phr*$^-$ cells growing in suspension. Figure 10B shows DAPI staining of both wild type and *phr*$^-$ cells at 0 hours (cells harvested from plates) and at 72 and 96 hours of growth in suspension. As can be seen in the figure, neither *phr*$^-$ cells nor wild-type cells are multi-nucleated on plates. Appearance of some multinucleated cells after 72 hours in suspension is observed in both phr$^-$ wild-type cells. Therefore, *phr*$^-$ cells do not appear to have growth nor cytokinesis defects.

phr$^-$ cells display delayed aggregation

The Sca1 complex was shown to control signal relay and therefore the aggregation of cells during development (Charest et al., 2010). The role of PHR in *Dictyostelium* development was assessed by a study of the phenotypic difference of *phr*$^-$ strains compared with wild-type cells and other Sca1 complex knockouts undergoing starvation-induced development. The images shown in Figure 11 show a delay in the development of *phr*$^-$ cells when compared to wild-type cells. *phr*$^-$ cells do not form mounds at 8h, as is typical for wild-type cells, but rather are delayed and form mounds at ~12h. However, *phr*$^-$ cells do complete their developmental program and form fruiting bodies at 24h after starvation. Aggregation and multi-cellular development of *phr*$^-$ strains seems to be only delayed, but not ultimately affected.

Within the context of other Sca1 complex mutants, the developmental phenotype of *phr*$^-$ cells is most comparable to that of *gefH*$^-$ cells. Note that both *phr*$^-$ and *gefH*$^-$ cells show delayed aggregation yet ultimately produce fruiting bodies, whereas *gefA*$^-$ and *scaA*$^-$ cells show almost no aggregation.

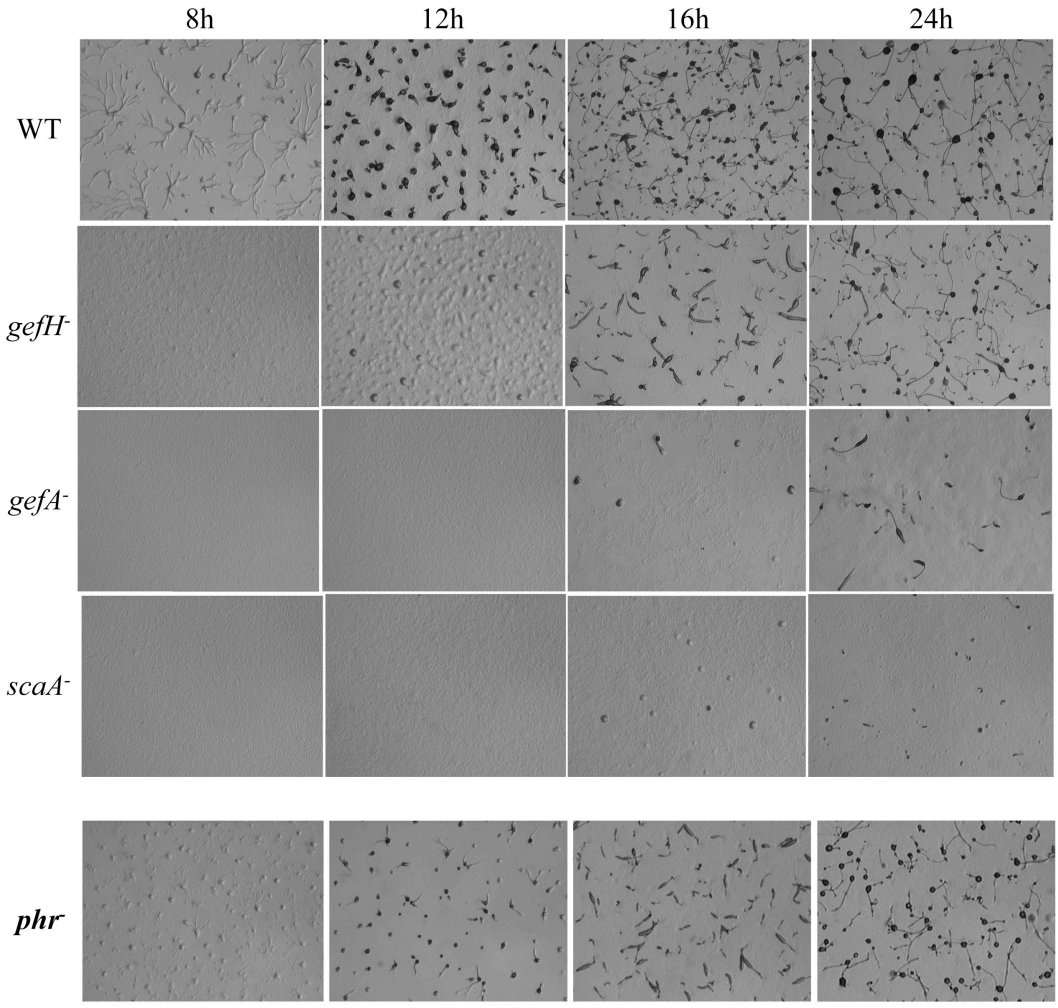

Figure 11. *Dictyostelium* development. Development of the different knockout strains compared to WT on non-nutrient Na/K agar plates. Times indicated refer to time picture taken after initial plating. Data representative of ≥ 3 independent experiments. For WT, *gefH*$^-$, *gefA*$^-$, and *scaA*$^-$ data taken with permission from Charest et al., 2010.

phr$^-$ cells exhibit chemotaxis defects but enhanced vegetative cell motility

Further characterization of the *phr*$^-$ strain was performed as cells were examined for chemotaxis or vegetative cell motility defects. When compared to wild-type cells, there is a noticeable defect in *phr*$^-$ cells chemotaxis (Figure 12). The *phr*$^-$ cells migrate more slowly and with less directionality than wild-type cells. This could be due to the

fact that the leading edge of *phr*⁻ cells tended to lift off of the substratum during chemotaxis with a higher frequency and for longer periods of time than that of wild-type cells (Video 2), suggesting a possible adhesion defect or cytoskeleton mis-regulation. Interestingly, the *phr*⁻ chemotaxis phenotype is much more severe than that of *gefH*⁻ cells, being most similar to that of *scaA*⁻ cells.

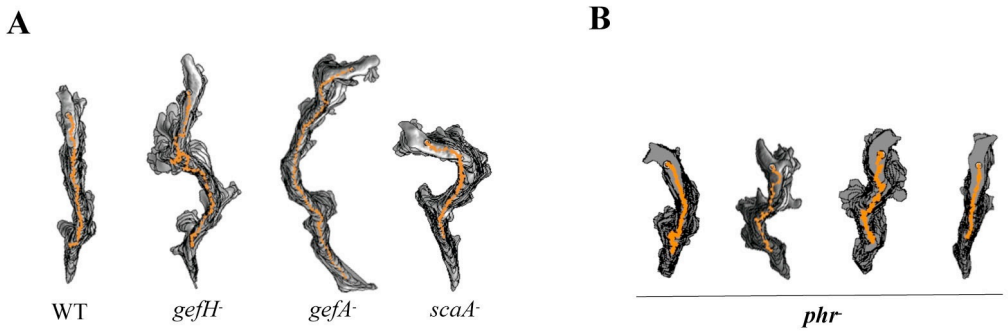

C

Strain	Speed (μm/min)	Directionality	Direction Change (deg)	Roundness (%)
WT	8.1 ± 2.7	0.86 ± 0.04	33 ± 9	35 ± 5
gefH⁻	9.4 ± 1.1	0.75 ± 0.10	36 ± 9	31 ± 7
gefA⁻	11.7 ± 2.5	0.78 ± 0.09	24 ± 8	32 ± 4
scaA⁻	8.0 ± 1.0	0.63 ± 0.08	39 ± 6	27 ± 2
phr⁻	6.9 ± 1.5	0.65 ± 0.12	35 ± 9	35 ± 6

Figure 12. Effect of gene disruption on chemotaxis. Individual tracings of representative developed **(A)** Sca1 complex mutants (Charest et al., 2010) and **(B)** *phr*⁻ cells performing chemotaxis towards cAMP. **(C)** DIAS analysis of *phr*⁻ cells was compared to WT cells and Sca1 complex mutants from Charest et al., 2010. Analysis performed on 10 traces from 3 independent experiments. Speed refers to the speed of the cell's centroid movement along the total path; Directionality indicated migration straightness; Direction change refers to the number of and frequency of turns; and Roundness indicates cell polarity.

To investigate if the severe chemotaxis defect of *phr*$^{-}$ cells results from a basic cell motility defect, the random motility of vegetative *phr*$^{-}$ cells was assessed and compared to that of wild-type cells. Interestingly, though *phr*$^{-}$ cells show reductions in chemotaxis within a cAMP gradient, they show a marked increase in random cell motility (Figure 13). PHR knockout cells display an increase in speed, persistence and cell polarity when compared to wild-type cells. Similarly, *phr*$^{-}$ cells display a reduction in direction change – consistent with the other observed phenotypes. This increased random motility observed for *phr*$^{-}$ cells greatly contrasts with that of the other Sca1 complex mutants, which display reduced motility compared to that of wild-type cells, and does not explain the severe chemotaxis defect of *phr*$^{-}$ cells.

Since PHR is brought into the Sca1 complex through interaction with RasGEFH, the drastically different phenotypes observed for *phr*$^{-}$ and *gefH*$^{-}$ cells might be indicative of a secondary role of PHR in the control of cell motility and chemotaxis, besides functioning within the Sca1 complex.

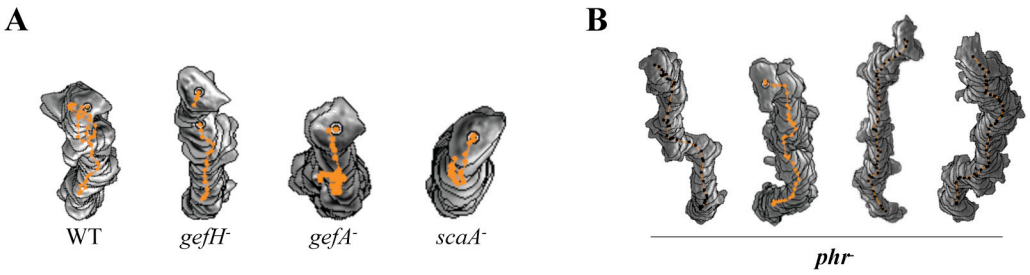

C

Strain	Speed (μm/min)	Persistence	Direction Change (deg)	Roundness (%)
WT	3.8 ± 1.3	0.43 ± 0.13	39 ± 7	59 ± 7
gefH$^-$	3.2 ± 1.3	0.46 ± 0.30	36 ± 7	62 ± 6
gefA$^-$	2.6 ± 1.7	0.27 ± 0.26	54 ± 17	61 ± 9
scaA$^-$	1.6 ± 0.7	0.15 ± 0.10	55 ± 9	69 ± 5
phr$^-$	5.9 ± 1.3	0.77 ± 0.24	26 ± 3	50 ± 4

Figure 13. Effect of gene disruption on random cell motility. Individual tracings of representative **(A)** Sca1 complex mutants (Charest et al., 2010) and **(B)** *phr*$^-$ randomly moving vegetative cells. **(C)** DIAS analysis of *phr*$^-$ cells was compared to WT cells and Sca1 complex mutants from Charest et al., 2010. Analysis performed on 10 traces from 3 independent experiments. Speed refers to the speed of the cell's centroid movement along the total path; Persistence indicates the persistence of movement in a given direction; Direction change refers to the number of and frequency of turns; and Roundness indicates cell polarity.

F-actin polymerization and Myosin assembly are elevated in *phr*$^-$ cells

Due to both the increase in vegetative cell motility and observed chemotaxis defects in *phr*$^-$ cells, the chemoattractant-induced modulation of the cytoskeleton in *phr*$^-$ cells was assessed. As presented in Figure 14, *phr*$^-$ cells exhibit a marked increase in both chemoattractant-induced myosin assembly (MyoII) and F-actin polymerization when compared to wild-type cells. After the initial decrease in MyoII, *phr*$^-$ cells display increased and prolonged chemoattractant-induced MyoII levels when compared to wild-type cells (Figure 14A). In terms of F-actin, *phr*$^-$ cells undergo a rapid increase in F-actin

polymerization at 5 seconds after cAMP stimulation, as seen in wild-type cells, but exhibit unique elevated and sustained chemoattractant-induced F-actin polymerization (Figure 14B).

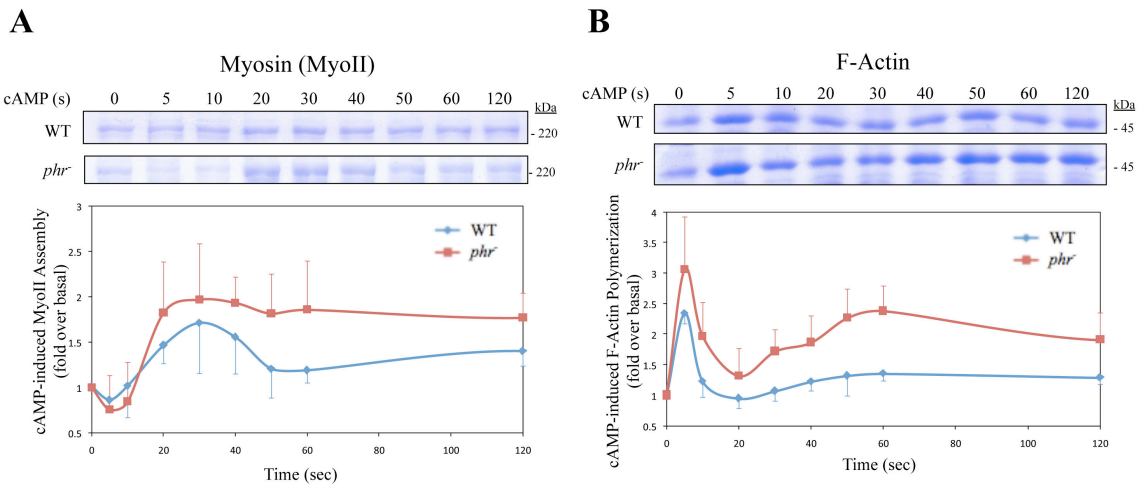

Figure 14. Cytoskeleton profiles of *phr*⁻ cells. Representative Coomassie blue-stained SDS-PAGE-resolved **(A)** Myosin II (MW: 220 kDa) and **(B)** F-actin (MW: 45 kDa) proteins of developed cells stimulated or not with 1µM cAMP for the times indicated in *phr*⁻ and WT cells. Graph shown represents data quantified using densitometry software, ImageGauge. All values were compared to 0" timepoint and are expressed as fold over basal. Vertical error bars represent the calculated SEM. Data representative of 4 independent experiments.

To further investigate the regulation of F-actin in *phr*⁻ cells, a phalloidin staining of both vegetative and developed cells was performed. Phalloidin binds to F-actin with very high affinity and is an excellent qualitative indicator of F-actin within the cell. As shown in Figure 15, there is a visible increase in F-actin levels in both vegetative and developed *phr*⁻ cells when compared to those in wild-type cells. In addition, vegetative *phr*⁻ cells show a visible increase in observed pseudopodia extension. This finding can explain the increase in the random cell motility of vegetative *phr*⁻ cells. Developed *phr*⁻

cells also show an increased basal level of F-actin, as shown by the strong signal at the leading edge of polarized cells.

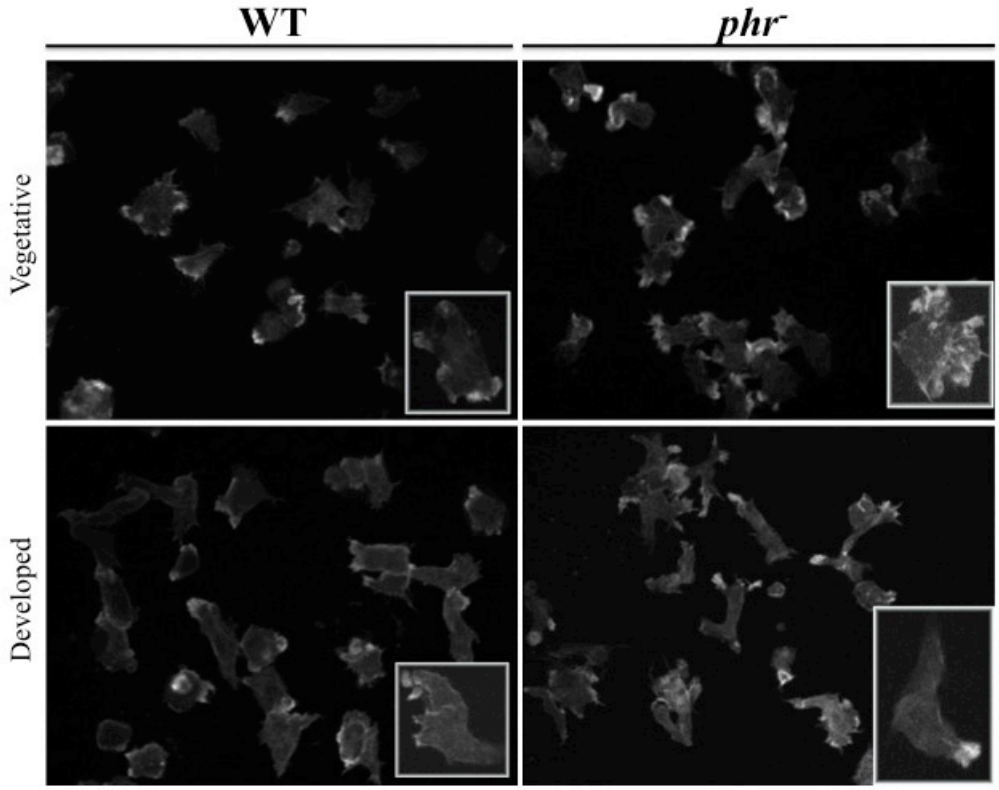

Figure 15. Qualitative analysis of F-actin polymerization in vegetative and developed *phr*⁻ and WT cells. Cells were stained with TRITC-labeled phalloidin and images were taken at 63X magnification. Individual representative cells of each condition are shown in higher magnification. Data representative of 3 independent experiments.

PHR is not involved in RasC activation but modulates TORC2 activity

The Sca1 complex is involved in the tight regulation of the RasC-TORC2 pathway (Charest et al., 2010). Therefore, a role for PHR in the regulation of this pathway was investigated. As shown in Figure 16, no considerable difference in chemoattractant-induced RasC activity is observed in *phr*⁻ cells compared to that in wild-type cells, suggesting that PHR is not involved in the activation of RasC by the Sca1

complex. TORC2 activity, via the TORC2-mediated phosphorylation of PKB and PKBR1 at their hydrophobic motifs, was then analyzed in *phr*$^-$ cells. Interestingly, as shown in Figure 17, *phr*$^-$ cells show a reduction in TORC2-mediated phosphorylation of PKB and PKBR1 when compared to that in wild-type cells. Together, these results suggest that PHR modulates the activity of TORC2 independently of RasC.

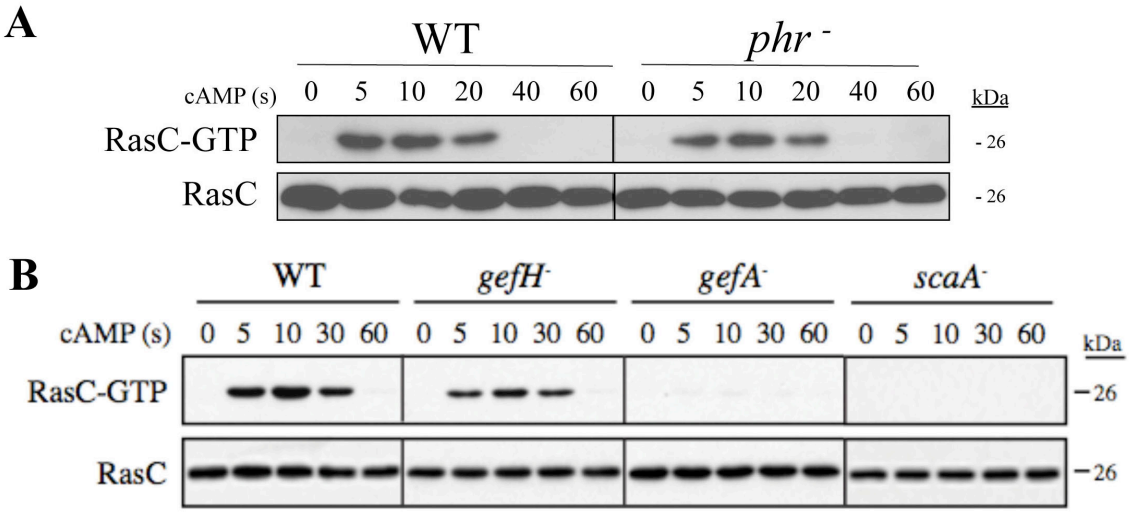

Figure 16. Regulation of RasC Activity in *phr*$^-$ cells . (A and B) Flag-RasC was expressed in the indicated strains and cAMP-induced RasC activity assessed via pull-down of active RasC (RasC-GTP) with GST-RBD (Byr2) at the indicated times after initial stimulation. Pulled-down and total RasC revealed by Flag immunoblot. **(B)** Adapted from Charest et al., 2010.

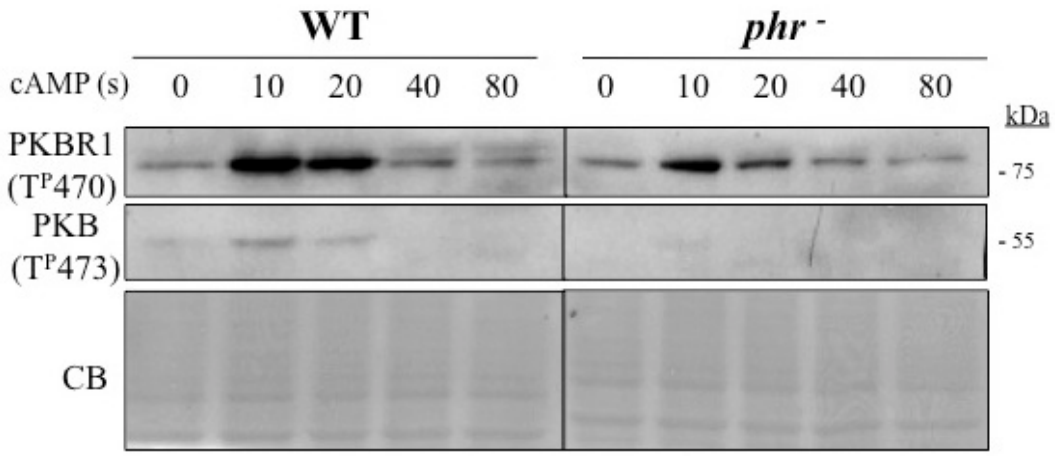

Figure 17. Effect of *phr* knockout on downstream TORC2-PKB/PKBR1 pathway. Representative SDS-PAGE-resolved immunoblots of phosphorylated PKBR1 and PKB (at threonine 473 (T^P473) and threonine 470 (T^P470), respectively). Total cell lysates were collected at indicated times after cAMP stimulation and incubated with antibody anti-p70S6K (1A5) for immunoblotting via HRP. Membranes were stained with Coomassie blue (CB) as a loading control. Data are representative of at least 5 independent experiments.

Attempts to clone and express PHR-tagged proteins

Several attempts to generate cells expressing epitope-tagged or GFP-fused PHR were made. The *phr* gene was cloned according to the gene model suggested by *dictyBase*. Initial attempts to generate cells expressing N-terminal His-HA-Flag (HHF)- and GFP-PHR constructs in *phr* null background were unsuccessful; western blotting of HHF-PHR/*phr*$^-$ cells showed no detectable expression of the protein and GFP-PHR-transformed *phr*$^-$ cells showed no fluorescence under microscopy. However, *phr*$^-$ cells expressing PHR with a C-terminal Flag-HA-His (FHH) tag (PHR-FHH) or GFP (PHR-GFP) were generated. Screening of PHR-GFP-expressing cells by fluorescence

microscopy revealed expression of the fusion protein in *phr*$^{-}$ cells and a western blot showing *phr*$^{-}$ clones expressing PHR-FHH is shown in Figure 18A.

In order to investigate potential proteins interacting with PHR independently of the Sca1 complex, a pull-down of PHR in the presence of a protein cross-linker was attempted. A sequential His-Flag purification was done with vegetative (V) and developed (D) PHR-FHH/*phr*$^{-}$ cells and wild-type cells as control. Alarmingly, there was no band at ~130 kDa, the expected size for PHR, in any of the pull-down samples (Figure 18B). Figure 4 shows the original pull-down performed by Charest et al. for comparison. This result is very surprising, because although PHR levels were lower than other Sca1 complex components in the original pull-down, there should be a very high signal at ~130kDa when PHR is used as bait.

The pull-down results suggested that something was happening to the tagged PHR protein. To investigate possible degradation of the PHR constructs, several western blots (anti-GFP and anti-HA, respectively) were performed on both vegetative (V) and developed (D) C-terminal tagged PHR-expressing cells. Soluble GFP and HHF-RasGEFH were used as positive controls for the Western blots. As can be seen in Figure 18C, most of the signal detected for the cells transformed with PHR-FHH or PHR-GFP is at very low molecular weight. This suggests that there is cleavage of the C-terminal tag or GFP fused to PHR. Due to the presence of some C-terminal tagged protein at the appropriate molecular weight, it can be speculated that there is some post-translational regulation of PHR occurring.

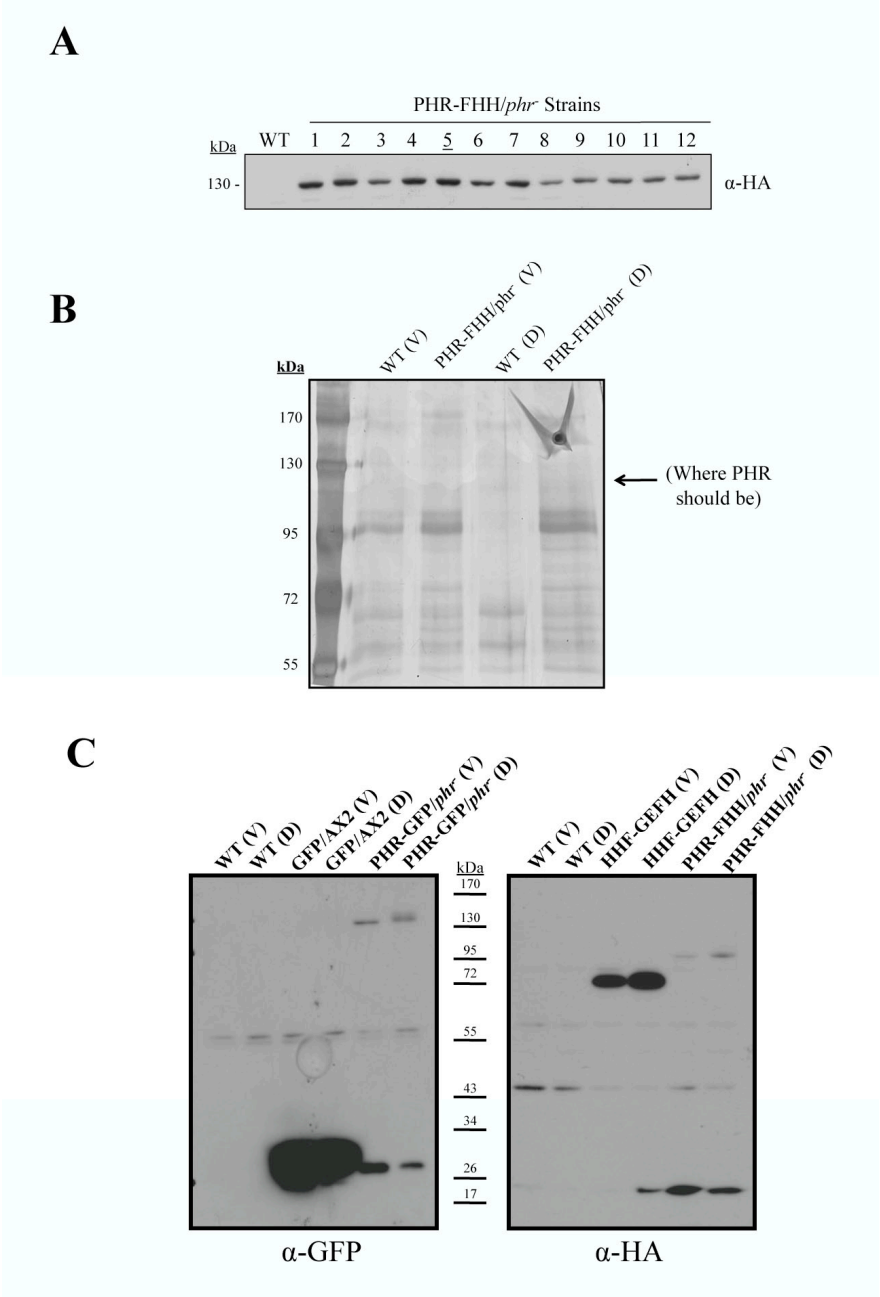

Figure 18. Attempts to clone epitope-tagged PHR proteins. (A) anti-HA immunoblot to screen potential C-terminal FHH-tagged PHR expressing *phr*⁻ cells. **(B)** Silver staining of a sequential His-Flag purification/pull-down experiment in FHH-PHR/*phr*- and WT cells. **(C)** SDS-PAGE-resolved immunoblots (anti-GFP and anti-HA) of several tagged-PHR expressing strains and controls under both vegetative (V) and developed (D) conditions. For **A** and **C,** proteins were quantified prior and 20ug was loaded for each sample.

As a result of the findings depicted in Figure 18C, combined with the previous difficulty of generating cells expressing N-terminally tagged PHR, and the inability to clone PHR from a cDNA library, contact was made with curators at *dictyBase*. Helped by our observations, the old gene model was negated and a new gene model was predicted. The two different gene models are shown in Figure 19. Note that the start sites of both gene models are very different, which can explain the previous failure to generate N-terminally-tagged constructs. However, cloning of the PHR cDNA according to the second gene model has also proved unsuccessful. To date, it is still unclear what the true start site of the *phr* gene is and what is happening with the protein's C-terminus.

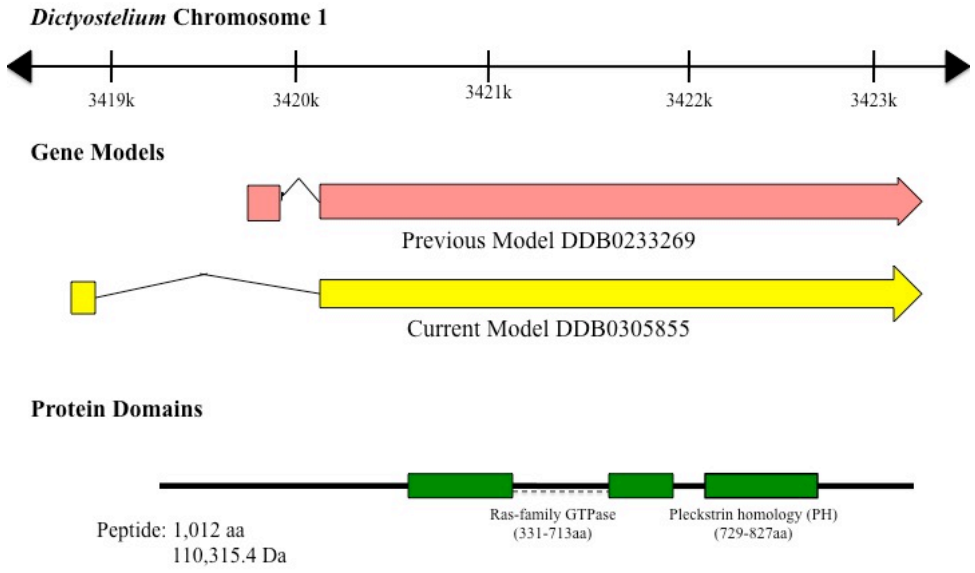

Figure 19. PHR Gene Models. As predicted by *dictyBase.* Protein domains shown in relation to gene models and chromosomal alignment.

III. DISCUSSION

As recently discovered by Charest et al. 2010, the Sca1 protein signaling complex is involved in the spatiotemporal regulation of chemotaxis and signal relay through activation of the RasC-TORC2-PKB/PKBR1 pathway at the leading edge of chemotaxing cells. PHR is a stable member of this complex, but experimental evidence suggests that it may also play a distinct role in regulating the cytoskeleton and chemotaxis.

This study demonstrates that *phr*$^{-}$ cells have distinct F-actin and Myosin II (MyoII) profiles when compared to other components of the Sca1 complex. Additionally, *phr*$^{-}$ cells exhibit severe chemotaxis defects; the decrease in speed and directionality is more severe than single *rasgefH*$^{-}$ mutants. This finding, coupled with the fact that RasGEFH recruits PHR to the Sca1 complex suggests that PHR regulates chemotaxis in a process that is distinct or parallel in function to the Sca1 complex. However, because the correct topology of the gene encoding PHR remains unknown, cloning a stable protein was more difficult than anticipated. Thus, the mechanisms by which PHR might regulate *Dictyostelium* cytoskeleton components and chemotaxis remain to be discovered.

Generation and morphology of a stable *phr-* strain

The generation of a stable *phr* knockout cell line was done using homologous recombination and the insertion of a Blastocidin S resistance (BSR) cassette to disrupt the gene. Once the knockout construct was transformed into *Dictyostelium* cells, the PCR screens and Southern Blot protocol were designed to confirm the correct gene disruption. Though the data from the Southern Blot does not provide absolute confirmation of *phr*

knockout, the data is considered more than sufficient proof when coupled with the three PCR screens (see Results).

The *phr*$^-$ cells in suspension grew at the same rate as that of wild-type cells. However, the *phr*$^-$ cells appeared bigger than wild-type cells when cultured on plates. The individual *phr* knockout cells appeared flatter and more spread out, perhaps alluding to abnormal adhesion. Other than the perceived size difference, the general morphology, growth rate, and cytokinesis of *phr*$^-$ cells were similar to that of wild-type cells. *phr* knockout appears to have no effect on the growth of cells, but perhaps on the cell's ability to adhere to a substratum.

phr knockout results in decreased chemotaxis, despite increased cytoskeleton

The most severe phenotype observed in *phr* knockout cells was the decrease in speed and directionality of chemotaxing cells. Chemotaxis is essential for *Dictyostelium* cells to complete a multi-cellular development program or to move towards a food source. In order for chemotaxis to occur there must be tight regulation and coordination of the cytoskeleton to allow for the directed movement of cells towards the chemical stimulus. A mis-regulation of either the F-actin or MyoII could underlie this chemotaxis defect. Interestingly, developed *phr*$^-$ cells exhibit elevated and sustained levels of F-actin and MyoII when compared with wild-type cells. Intriguingly, there is a coincidence of elevated F-actin levels in developed *phr*$^-$ cells that also display very evident chemotaxis defects. One possible explanation for the chemotaxis defects observed in developed *phr*$^-$ cells is the fact that *phr*$^-$ cells tended to lift off of the substratum more frequently and for longer durations than wild-type cells. A potential adhesion defect in the null cells could

explain the paradox between the chemotaxis defects observed and elevated levels of cytoskeleton; if *phr*$^{-}$ cells have increased cytoskeleton, but exhibit parallel adhesion defects, the cell's ability to undergo chemotaxis would be inhibited, as chemotaxis requires optimal adhesion for both protrusion and retraction.

Interestingly, Rap1-null cells show elevated levels of F-actin in developed cells and exhibit chemotaxis defects. Cellular adhesion defects account for the observed decrease in chemotaxis of Rap1 null cells (Jeon et al., 2007). Rap small GTPases are part of the Ras superfamily of small GTPases and are primarily associated with the regulation of the cytoskeleton (Charest and Firtel 2007). This data on both Rap1 adhesion and chemotaxis defects, along with elevated F-actin levels in Rap1 null cells, supports the idea that an adhesion defect could be the cause of the decreased speed and directionality observed in chemotaxing *phr*$^{-}$ cells. A direct comparison of the adhesion maintenance of *phr*$^{-}$ cells and *rap1*$^{-}$ cells could help confirm or deny that adhesion defects are causing *phr* null cells' chemotaxis defects. Alternatively, as PHR contains a small GTPase domain, it is possible that PHR could act as an atypical Rap small GTPase. This hypothesis remains to be tested.

Intriguingly, despite evident chemotaxis defects, vegetative *phr*$^{-}$ cells have increased random cell motility. Vegetative *phr*$^{-}$ cells move with more speed, persistence, and polarity when compared to wild-type cells and other Sca1 complex mutants. The increased vegetative motility of *phr*$^{-}$ cells is supported by the observation of elevated F-actin and pseudopod extensions in the vegetative null strains.

Effect of *phr* knockout on delayed aggregation

The marked reductions in speed and directionality in chemotaxing *phr*$^-$ cells can explain the observed delay in aggregation. These chemotaxis defects appear to be related to the mis-regulation of the cytoskeleton and cellular motility machinery, or to possible abnormal adhesion. However, this delay in aggregation could also be the result of altered intracellular signaling that controls Signal Relay in the null cells. This study did not assay the cAMP production in *phr*$^-$ cells, but does not exclude the possibility that PHR might affect signal relay, either within the Sca1 complex or in a parallel pathway. To rule out any effect PHR might have on Signal Relay, an assay of ACA activity and cAMP production (per Charest *et al.*, 2010) would be compared to *rasgefH*$^-$ mutants and wild-type cells; if the observed phenotype is different in *phr*$^-$ cells than in *rasgefH*$^-$ cells, it can be assumed that PHR may affect Signal Relay. However, since *phr*$^-$ cells show no detectable effect on RasC activity, it can be postulated that PHR does not play a large role in modulating ACA function and cAMP production.

PHR modulates TORC2 activity, independently of RasC and the Sca1 Complex

Interestingly, though data suggests that RasGEFH recruits PHR to the Sca1 complex (Charest et al., 2010), the unequal chemotaxis and vegetative cell motility phenotypes of *phr*$^-$ and *rasgefH*$^-$ cells can be indicative of other functions of PHR in regulating chemotaxis outside of the Sca1 complex. Alternatively, PHR could play a very intricate and complicated role in the regulation of the complex.

Though PHR knockout has no detectable effect on RasC activity, it does appear to modulate TORC2 activity, seen through a reduction in the TORC2-mediated

phosphorylation of the hydrophobic motifs (HM) of PKB/PKBR1. However, this is not a direct assay of TORC2 kinase activity. This study, at present, does not rule out that the observed reduction in the phosphorylation of PKB/PKBR1 HMs could be due to the mis-regulation of a phosphatase in *phr*$^{-}$ cells. For this reason, it is suggested that an assay that directly measures the kinase activity of TORC2 be developed for use on *phr*$^{-}$ cells. If found that PHR knockout does directly modulate the kinase activity of TORC2, the mechanism by which it acts would still remain unknown. Since PHR has a GTPase domain, perhaps PHR binds directly to components of the TORC2 complex. A Y2H of PHR with Ras interacting protein 3 (Rip3), a component in the TORC2 complex with a Ras-binding Domain (RBD) known to bind other small GTPases, would test for this direct interaction between PHR and the TORC2 complex.

Alternatively, PHR could modulate TORC2 function in a pathway parallel to the Sca1-RasC-TORC2 pathway – it could be implicated in the potential regulation of TORC2 by RasG. As discovered by Kamimura et al., there is residual TORC2 activity in *rasC*$^{-}$ cells, suggesting that TORC2 is only partially controlled by RasC. This finding, coupled with the discovery that the Rip3 interacts with RasG *in vitro* (Lee et al., 1999), allows for the possibility that TORC2 is controlled by several parallel pathways: by both RasC and RasG, or perhaps other regulators. If PHR is implicated in mechanisms outside of the Sca1 complex, it may control TORC2 activity through interactions with RasG and/or PI(3,4,5)P_3-PI3K. As stated previously, Bolourani et al. delineated distinct functions for RasG and RasC *in vivo* for *Dictyostelium*: they noticed that RasG was more important in the regulation of chemotaxis, and RasC regulated ACA activity and cAMP Signal Relay. This evidence, together with the finding that the Sca1 complex promotes

RasC activation at the leading edge of developed cells in regions that are also enriched with chemoattractant-stimulated RasG-GTP (Charest et al., 2010), promotes the hypothesis that PHR might have dual and parallel functions in both the RasG and RasC pathways. Whereas PHR might be necessary for Sca1 localization to the leading edge for RasC activation (Charest et al., 2010), perhaps through phospholipid-binding, there it could co-promote the RasG-PI3K-PKB pathway to control cell polarity and motility.

To test the possibility that PHR is a component in the PI(3,4,5)P_3-PI3K-RasG pathway, an analysis of what phospholipids PHR preferentially binds through its PH-domain should be performed. If PHR does interact with PI(3,4,5)P_3, then further investigation into the role of PHR in the RasG-PI3K pathway should be done. For example, localization studies using fluorescent reporters such as the PH domain of the cytosolic regulator of adenylyl cyclase fused to GFP (GFP-PH_{CRAC}) to test chemoattractant-stimulated PI3K activity, or GFP-Raf1RBD (a RasG activity reporter) could be done in *phr*$^-$ cells to observe any spatiotemporal disruption of this RasG-PI3K-PI(3,4,5)P_3 pathway. Additionally, in the study by Bolourani et al., it was found that *rasG*$^-$ cells also have decreased PKB activation. Another way to test the possible involvement of PHR in the RasG-PI3K-PI(3,4,5)P_3 pathway would be to analyze lysates of cAMP-stimulated developed cells by Western blotting using a phospho-threonine-specific antibody that is capable of detecting the phosphorylation of PKB (Lim et al., 2001). A similar decrease in PKB phosphorylation in *phr*$^-$ cells could indicate a function of PHR upstream of RasG in the RasG-PI3K-PKB pathway.

.

Further Experimentation with PHR

Due to the fact that *phr*$^{-}$ cells displayed elevated levels of F-actin and MyoII, further investigation is needed to better understand the cytoskeleton dynamics in the null cells. I propose live cell imaging of *phr*$^{-}$ cells using fluorescent reporters, such as LimEΔcoil (Zhang, 2008) or Myosin-GFP. This imaging could be done with each separate reporter, or with both reporters co-expressed in the same cell.

Additionally, as adhesion defects may underlie the observed chemotaxis defects observed in *phr*$^{-}$ cells, an investigation into possible adhesion abnormalities should be done per the Adhesion Maintenance studies performed in Fey et al., 2006 and Kowal, 2011.

In order to investigate other possible functions of PHR, the generation of epitope-tagged PHR-expressing cells is necessary. First, I suggest cloning PHR from a cDNA library using gene-specific primers, engineered to amplify the N- and C-terminus of both gene models as well as only the second exon. As the true start site of the PHR gene is unknown, the ability to successfully amplify the gene from a cDNA library is the first step in elucidating any additional functions of PHR. Once a stable strain of HHF-tagged PHR-expressing cells is generated, a sequential His-Flag purification would be needed to look into any other proteins that interact with PHR.

Once the gene model for PHR is known, then structural-function studies of the protein could also be performed. Analysis of the functionality of PHR's GTPase domain could provide insight into how PHR regulates cell motility and chemotaxis – whether as an independent small GTPase, or in concert with other signaling proteins. The purpose of this assay is to see if PHR's GTPase is activated by chemoattractant. Comparing the

kinetics of PHR's GTPase activity with other known small GTPases (e.g. Ras or Rap) could give important clues to the function of PHR in regulating the cytoskeleton and chemotaxis. Additionally, localization studies using fluorescent-labeled PHR will also prove useful in determining the function of PHR and its role in the spatiotemporal regulation of chemotaxis. Other structure-function studies can include a deletion series of the PHR protein. These deletion mutants can be used in biochemical assays as well as localization studies to further investigate PHR's role within the *Dictyostelium* cell.

Conclusions

Understanding the roles and function of PHR is necessary to further our understanding of the complex signaling network that regulates directed cell migration. Understanding the functions of PHR can also have greater implications, as it may aid in the development of new drug therapies to treat inflammatory diseases, cancer metastasis, and other disorders involving deregulated cell motility and chemotaxis.

IV. MATERIALS AND METHODS

Plasmid Constructs and Cloning

Standard protocol was followed for all PCR, restriction digest, agarose gel purification, ligation and bacterial transformation. All restriction enzymes and corresponding buffers used were from New England Biolabs or Invitrogen. Plasmids used were: pBlueScript (SK-) to clone in *E. Coli* (XL-1 Blue and DH5α cells); and pEXP4+ to transform into *Dictyostelium* cells. All constructs were sequenced for accuracy.

To generate a knockout construct for PHR, two non-overlapping gene fragments were amplified using PCR and ligated into pBlueScript (pBS) vector. Fragment PHR "A" was derived from PHR genomic DNA (PHRgDNA) from position 1149 to 2177. Fragment PHR "B" was made from the genomic sequence between 3662 and 4572 nucleotides. Each fragment contains a BamHI site: PHR "A" at its C-terminus and PHR "B" at its N-terminus (Figure 7). This PHR-A/B-pBS vector was then digested with BamHI, to allow for the insertion of a Blasticidin S Resistance (BSR) cassette, which was cut from a pLPBLP vector (Faix et al., 2004) using its flanking N- and C-terminus BamHI sites. This PHR-A(BSR)B-pBS construct was sequenced for accuracy before linearization using restriction enzymes KpnI and NotI for transformation into *Dictyostelium*. The BSR cassette was inserted between nucleotides 2177 and 3662 of the *phr* genomic sequence.

To generate epitope-tagged PHR or GFP-fusion expression constructs: HHF (His-HA-Flag) or GFP sequences were inserted in frame either in front of or downstream of PHRgDNA by PCR, with a minimum of 3 aa linker. These epitope-tagged PHR

fragments were then inserted into pEXP4+, containing the neomycin-resistance genes, for expression in *Dictyostelium*.

Cell Culture

Both wild-type (AX2) and *phr*$^-$ strains were maintained in HL5 medium either in suspension or on 100mm plates.

For transformation into *Dictyostelium* cells, cells were grown in shaking culture overnight and re-suspended in electroporation buffer (12mM Na/KPO_4 Buffer and 50mM Sucrose) to a final concentration of $10x10^6$ cells/ml. To generate the *phr*$^-$ knockout strain, 0.8mL of wild-type cells were mixed on ice with 30µg of linear PHR-A(BSR)B in 4mm electroporation cuvettes. The electroporation was done using a Bio-Rad Gene Pulser (with settings: 1kV, 3µF and a λ of 0.7-0.9). Each sample was pulsed twice. Electroporated cells were plated on 100mm dishes with HL5 medium. Clones were selected in 7.5µg/ml Blastocidin S.

When transforming PHR-tagged or Flag-tagged RasC constructs into *Dictyostelium*, the same procedure was done in its entirety, save for the use of 20µg of plasmid DNA transformed into wild-type or *phr*$^-$ cells. Clones were selected with and maintained in 20 ug/ml Geneticin, G418 (GIBCO)-supplemented HL5 medium.

Once grown to confluency on 100mm plates, the transformed cells were then re-suspended and mixed with ~2cm of plated *Klebsiella areogenes* (KA) or live E. coli B/r bacteria and plated on nutrient-agar plates to isolate clones. Once plaques formed they were individually picked and allowed to grow in selection media until screened.

Unless otherwise states, all assays were performed on aggregation-competent developed cells. To generate developed cells, each strain was grown in suspension for 24 hours prior to assay, washed and re-suspended in 12 mM Na/K phosphate buffer to a final concentration of $5x10^6$ cells/ml. Development was induced by pulsing the cells with 30nM cAMP final every 6 minutes for 5.5 hours in the 12mM Na/K phosphate starvation buffer pH 6.1.

Southern Blot

Genomic DNA (gDNA) was harvested from *Dictyostelium* cells using the PureGene Kit from Gentra Systems. gDNA was then restriction digested under two conditions: 1.) using enzymes EcoR1, PacI, and PmlI; 2.) EcoR1 and PmlI. Fragments were separated on agarose gel and transferred to nylon membrane. Southern was performed using a 630bp probe, generated from MscI and SpeI restriction digest of the knockout construct, spanning from nucleotides 3922 to 4552 of the PHRgDNA sequence.

Cytokinesis Assay and DAPI Staining

Cells were grown in suspension, with an initial concentration of $2x10^5$ cells/ml. Cell growth was assessed by counting the cells growing in suspension, using a hemocytometer, every 24-hours for 4 days. For nuclei staining, $1x10^6$ cells were allowed to adhere to a cover slip and were fixed in 3.7% formaldehyde/NaK phosphate buffer before staining with Hoescht stain in mounting media on microscope slides. Images were taken of the cells at 63X magnification.

Developmental Assays

Cells were grown overnight in suspension then washed and re-suspended in 12mM Na/K phosphate buffer to a final concentration of $2.0x10^7$ cells/ml. Then a 50µl drop was plated on a Na/K phosphate agar plate. Five 1:2 serial dilutions of the cells were made on the Na/K phosphate agar plates. Images were taken every 4 hours after the initial plating, for a period of 24 hours.

Chemotaxis Assay

Developed cells were re-suspended in 12mM Na/K phosphate buffer, in the absence of cAMP, and allowed to adhere to a cover-slip in a 30mm petri dish for ~20-30 minutes. A micropipette filled with 150µM cAMP was then placed in the petri dish, and images of the cells chemotaxing towards the cAMP diffusing from the micropipette were taken every six seconds for ≥ 100 frames using time-lapsed imaging. Data were generated using tracings of individual cells from the time-lapsed images and DIAS software.

For the analysis of vegetative cell motility, cells were harvested directly from plates and $0.3x10^6$ cells/ml were added directly to 3mL of 12mM Na/K phosphate starvation buffer in 30mm petri dishes, and allowed to adhere for ~20 minutes. After two washes with starvation buffer, cells were then continued to starve for 1 hour in the Na/K phosphate buffer. Images of the cells randomly moving were taken at 6-second intervals after starvation, over a course of 30 minutes, and were quantified using DIAS software and individual tracings from the time-lapsed images.

Actin and Myosin Assays

Cells were grown overnight in suspension, washed and re-suspended in starvation buffer (20mM MES pH 6.8, 0.2mM $CaCl_2$, and 2mM $MgSO_4$), and $5x10^6$ cells/ml of both cell lines were pulsed with 30nM cAMP final for 5.5 hours in starvation buffer. After pulsing, cells were shaken at room temperature for 20 minutes. Finally, cells were stimulated or not with 1μM cAMP and samples were collected at the indicated time and added to equal amount of 2X lysis buffer (20mM TES pH 6.8, 1% Triton X-100, 2mM $MgCl_2$, 5mM EGTA, 2ug/ml Aprotinin and Leupeptin). The Triton X-100 insoluble fractions were isolated and resolved on 7.5% SDS-PAGE. The polyacrylamide gels were then stained with Coomassie Blue. The bands representing Myosin II (220kDa) and F-actin (45kDa) were quantified by densitometry using the ImageGauge software.

Phalloidin Staining

$0.25x10^6$ cells were put onto cover slips in 6-well plates and allowed to adhere and spread for ~1h. Cells were fixed with 7.4% formaldehyde/NaK phosphate buffer for 10 minutes. Cells were then permeabilized with 0.2% Triton-X/PBS for 10 minutes. Cells were washed 3x with 3ml PBS for 5 minutes each before staining with TRITC-labeled Phalloidin in a moist chamber at room temperature for 30 minutes. Cells were washed 3x with 3ml PBS in the 6-wells plates and then cover slips were mounted on to slides. Images were taken using both 63X and 100X objectives.

RasC Assay

Flag-tagged RasC was transformed into both *phr*- and WT backgrounds and confirmed by Immunoblot prior to RasC Assay. Developed cells were stimulated or not with 100 nM cAMP for the indicated time. Aliquots were collected and added to 2X lysis buffer (100mM Tris pH 7.5, 300mM NaCl, 50mM $MgCl_2$, 20% glycerol, 1% NP-40, 2mM DTT, 2mM Vanadate, 2 ug/ul Aprotinin and Leupeptin). Samples were incubated on ice for 10 minutes before clearing by centrifugation. The supernatant was transferred to new tubes, on ice. For Total Ras measurement, 20ul of lysate was added to 20ul of 2X Sample Buffer. The remaining lysates were incubated on a rocker with 10ug of GST-fused Ras Binding Domain (GST-RBD) on glutathione-agarose beads and 2mg/ml BSA at 4°C for 30 minutes. The beads were then washed 3x with Lysis Buffer before elution in 1X Sample Buffer. Ras proteins were separated on 12% SDS-PAGE and transferred to Immobilon membrane before detection by Flag Immunoblot using anti-Flag M2 antibody and revealed by autoradiography

TORC2 activity assay [Phosphorylation of PKBR1 (T470) and PKB (T473)]

Developed cells were stimulated or not with 100nM cAMP final, and aliquots of cells were collected and directly lysed in Laemmli sample buffer. Samples were resolved on 8% SDS-PAGE, transferred to an Immobilon membrane, and analyzed by immunoblot using anti-p706SK antibody (1A5) that specifically recognizes the phosphorylated hydrophobic motifs of *Dictuyostelium* PKB and PKBR1. Coomassie Blue (CB) staining of the membrane was used for loading control.

REFERENCES

Affolter, M. and C.J. Weijer (2005). "Signaling to cytoskeletal dynamics during chemotaxis." Dev. Cell **9**:19–34.

Boguski, M.S., and F. McCormick (1993). "Proteins regulating Ras and its relatives." Nature. **366**: 643-654.

Bolourani, P., G.B. Spiegelman and G. Weeks (2006). "Delineation of the roles played by RasG and Ras C in cAMP-dependent signal transduction during the early development of *Dictyostelium discoideum*. Mol. Biol. Cell **17**: 4543-4550.

Bourne, H.R., D.A. Sanders, and F. McCormick (1991). "The GTPase superfamily: conserved structure and molecular mechanism. Nature **349**: 117-127.

Cantley, L. C. (2002). "The phosphoinositide 3-kinase pathway." Science **296**: 1655-1657.

Cenni, V., A. Sirri, M. Riccio, G. Lattanzi, S. Santi, A. de Pol, N. M. Maraldi and S. Marmiroli (2003). "Targeting of the Akt/PKB kinase to the actin skeleton." Cell. Mol. Life Sci. **60**: 2710-2720.

Charest, P.G. and R.A. Firtel (2007). "Big roles for small GTPases in the control of directed cell movement." Biochem. J. **401**: 377-390.

Charest, P.G., Z. Shen, A. Lakoduk, A.T. Sasaki, S.P. Briggs, R.A. Firtel (2010). "A Ras signaling complex controls the RasC-TORC2 pathway and directed cell migration." Dev. Cell **18**(5)**:** 737-749.

Chisholm, R.L. and R.A. Firtel (2004). "Insights into morphogenesis from a simple developmental system." Nature Rev. Mol. Cell Biol. **5**: 531-541.

Chung, C.Y. and R.A. Firtel (1999). "PAKa, a putative PAK family member, is required for cytokinesis and the regulation of the cytoskeleton in *Dictyostelium discoideum* cells during chemotaxis." J. Cell Biol. **147**: 559-576.

Colicelli, J. (2004). "Human RAS superfamily proteins and related GTPases." Sci. STKE 2004, RE13

Eichinger, L., J.A. Pachebat, G. Glöckner, M.-A. Rajandream, R. Sucang, M. Berriman, J. Song, R. Olsen, K. Szafranski, Q. Xu, B. Tunggal, S. Kummerfeld, M. Madera, B.A. Konfortov, F. Rivero, A.T. Bankier, R. Lehmann, N. Hamlin, R. Davies, P. Gaudet, P. Fey, K. Pilcher, G. Chen, D. Saunders, E. Sodergren, P. Davis, A. Kerhornou, X. Nie, N. Hall, C. Anjard, L. Hemphill, N. Bason, P. Farbrother, B. Desany, E. Just, T. Morio, R. Rost, C. Churcher, J. Cooper, S. Haydock, N. van Driessche, A. Cronin, I. Goodhead, D. Muzny, T. Mourier, A. Pain, M. Lu, D. Harper, R. Lindsay, H. Hauser, K. James, M. Quiles, M. Madan Babu, T. Saito, C. Buchrieser, A. Wardroper, M. Felder, M. Thangavelu, D. Johnson, A. Knights, H. Loulseged, K. Mungall, K. Oliver, C. Price, M.A. Quail, H. Urushihara, J. Hernandez, E. Rabbinowitsch, D. Steffen, M. Sanders, J. Ma, Y. Kohara, S. Sharp, M. Simmonds, S. Spiegler, A. Tivey, S. Sugano, B. White, D. Walker, J. Woodard, T. Winckler, Y. Tanaka, G. Shaulsky, M. Schleicher, G. Weinstock, A. Rosenthal, E.C. Cox, R.L. Chisholm, R. Gibbs, W.F. Loomis, M. Platze, R.R. Kay, J. Williams, P.H. Dear, A.A. Noegel, B. Barrell and A. Kuspa (2005). "The genome of the social amoeba *Dictyostelium discoideum*." Nature. **435**: 43-57.

Fey, P., S. Stephens, M. A. Titus, and R. L. Chisholm (2002). "SadA, a novel adhesion receptor in *Dictyostelium*." J. Cell Biol. **159**, 1109-1119.

Funamoto, S., R. Meili, S. Lee, L. Parry and R.A. Firtel (2002). "Spatial and temporal regulation of 3-phosphoinositides by PI 3-kinase and PTEN mediates chemotaxis." Cell **109**: 611-623.

Gilbert, S. (2006). "Developmental Biology, Eighth Edition, Sinauer Associates Inc, Sunderland MA." Pg 36.

Iijima, M. and P. Devreotes (2002). "Tumor suppressor PTEN mediates sensing of chemoattractant gradients." Cell **109**: 599-610.

Iijima, M., Y.E. Huang and P. Devreotes (2002). "Temporal and spatial regulation of chemotaxis." Dev. Cell **3**: 469–478.

Insall, R.H., J. Borleis and P.N. Devreotes (1996). "The Aimless RasGEF is required for processing of chemotactic signals through G-protein-coupled receptors in *Dictyostelium*." Curr. Biol. **6**: 719-729.

Janetopoulos, C., T. Jin, and P. Devreotes (2001). "Receptormediated activation of heterotrimeric G-proteins in living cells." Science **291**: 2408–2411.

Jeon, T.J., D. Lee, S. Lee, G. Weeks and R.A. Firtel (2007). "Regulation of Rap1 activity controls cell adhesion at the front of chemotaxing cells." Jour Cell Biol. **179**: 833-843.

Jin, T., N. Zhang, Y. Long, C.A. Parent and P.N. Devreotes (2000). "Localization of the G protein betagamma complex in living cells during chemotaxis." Science **287**: 1034-1036.

Kamimura, Y., Y. Xiong, et al. (2008). "PIP3-independent activation of TorC2 and PKB at the cell's leading edge mediates chemotaxis." Curr Biol **18**(14): 1034-1043.

King, J. S. and R. H. Insall (2009). "Chemotaxis: finding the way forward with Dictyostelium." Trends Cell Biol **19**(10): 523-530.

Kölsch, V., P.G. Charest and R.A. Firtel (2008). "The regulation of cell motility and chemotaxis by phospholipid signaling." J. Cell Sci. **121**: 551-559.

Kortholt, A. and P. J. van Haastert (2008). "Highlighting the role of Ras and Rap during *Dictyostelium* chemotaxis." Cell Signal. **20**(8): 234-239.

Kowal, A. and R.L. Chisholm (2011). "Uncovering a role for the tail of the *Dictyostelium discoideum* SadA protein in cell-substrate adhesion." Euk. Cell **10**(5): 662-671.

Lee, S., C.A. Parent, R. Insall and R.A. Firtel (1999). "A novel Ras-interacting protein required for chemotaxis and cyclic adenosine monophosphate signal relay in *Dictyostelium*." Mol. Biol. Cell **10**: 2829-2845.

Lee, S., F.I. Comer, A. Sasaki, I.X. Mcleod, Y. Duong, K. Okumura, J.R. Yates III, C.A. Parent and R.A. Firtel (2005). "TOR complex 2 integrates cell movement during chemotaxis and signal relay in *Dictyostelium*." Mol. Biol. Cell **16**: 4572-4583.

Lim, C.J., Spiegelman, G.B., and G. Weeks (2001). "RasC is required for optimal activation of adenylyl cyclase and Akt/PKB during aggregation." EMBO J. **20**: 4490-4499.

Manahan, C. L., P. A. Iglesias, Y. Long and P. N. Devreotes (2004). "Chemoattractant signaling in *Dictyostelium discoideum*." Annual Review of Cell and Developmental Biology **20**(1): 223-253.

Mondal, S., D. Bakthavatsalam, P. Steimle, B. Gassen, F. Rivero, A.A. Noegel (2008). "Linking Ras to myosin function: RasGEF Q, a *Dictyostelium* exchange factor for RasB, affects myosin II functions." J. Cell Bio. **181**(5): 747-760.

Parent, C. A. and P. N. Devreotes (1999). "A cell's sense of direction." Science **284**(5415): 765-70.

Rodriguez-Viciana, P., C. Sabatier, and F. McCormick (2004). "Signaling specificity by Ras family GTPases is determined by the full spectrum of effectors they regulate." Mol. Cell. Biol. **24**: 4943-4954.

Sarbassov, D.D., D.A. Guertin, S.M. Ali, and D.M. Sabatini (2005). "Phosphorylation and regulation of Akt/PKB by the Rictor-mTOR complex." Science. **307**: 1098-1101.

Sasaki, A.T., C. Chun, K. Takeda and R.A. Firtel (2004). "Localizaed Ras signaling at the leading edge regulates PI3K, cell polarity, and directional cell movement. J. Cell Biol. **167**: 505-518.

Sasaki, A.T. and R.A. Firtel (2006). "Regulation of chemotaxis by the orchestrated activation of Ras, PI3K, and TOR." Eur. J. Cell Biol. **85**: 873–895.

Weeks, G. P. Gaudet, and R.H. Insall (2005). "The small GTPase superfamily." In: *Dictyostelium* Genomics, ed. W.F. Loomis and A. Kusppa, Norfold, UK: Horizon Bioscience, 211-234.

Weeks, G. and G.B. Spiegelman (2003). "Roles played by Ras subfamily proteins in the cell and developmental biology of microorganisms." Cell Sig. **15**: 901-909.

Wennerberg, K., K.L. Rossman and C.J. Der (2005). "The Ras superfamily at a glance." J. Cell Sci. **118**: 843-846.

Xiao, Z., N. Zhang, D.B. Murphy and P.N. Devreotes (1997). "Dynamic distribution of chemoattractant receptors in living cells during chemotaxis and persistent stimulation." J. Cell Biol. **139**, 365–374.

Zhang, S, P.G. Charest and R.A. Firtel (2008). "Spatio-temporal regulation of Ras activity provides directional sensing." Curr. Biol. **18**(20): 1587-1593.